Journal of Physics: Condensed Matter

PAPER

Superconducting properties and μSR study of the noncentrosymmetric superconductor $Nb_{0.5}Os_{0.5}$

To cite this article: D Singh *et al* 2018 *J. Phys.: Condens. Matter* **30** 075601

IOP Publishing Journal of Physics: Condensed Matter
J. Phys.: Condens. Matter **30** (2018) 075601 (8pp) https://doi.org/10.1088/1361-648X/aaa376

Superconducting properties and μSR study of the noncentrosymmetric superconductor $Nb_{0.5}Os_{0.5}$

D Singh[1], J A T Barker[2], A Thamizhavel[3], A D Hillier[4], D McK Paul[2] and R P Singh[1]

[1] Indian Institute of Science Education and Research Bhopal, Bhopal, 462066, India
[2] Physics Department, University of Warwick, Coventry CV4 7AL, United Kingdom
[3] Department of Condensed Matter Physics and Materials Science, Tata Institute of Fundamental Research, Mumbai 400005, India
[4] ISIS Facility, STFC Rutherford Appleton Laboratory, Harwell Science and Innovation Campus, Oxfordshire, OX11 0QX, United Kingdom

E-mail: rpsingh@iiserb.ac.in

Received 13 November 2017, revised 20 December 2017
Accepted for publication 21 December 2017
Published 22 January 2018

Abstract

The properties of the noncentrosymmetric superconductor (α-Mn structure) $Nb_{0.5}Os_{0.5}$ have been investigated using resistivity, magnetization, specific heat, and muon spin relaxation and rotation (μSR) measurements. These measurements suggest that $Nb_{0.5}Os_{0.5}$ is a weakly coupled ($\lambda_{e-ph} \sim 0.53$) type-II superconductor ($\kappa_{GL} \approx 61$), having a bulk superconducting transition temperature $T_c = 3.07$ K. The specific heat data fits well with the single-gap BCS model indicating nodeless s-wave superconductivity in $Nb_{0.5}Os_{0.5}$. The μSR measurements also confirm s-wave superconductivity with the preserved time-reversal symmetry.

Keywords: noncentrosymmetric superconductors, μSR, unconventional superconductors

(Some figures may appear in colour only in the online journal)

1. Introduction

Understanding the mechanism of unconventional superconductivity, where the structure lacks an inversion symmetry has been a tough challenge ever since the discovery of the heavy fermion noncentrosymmetric (NCS) superconductor $CePt_3Si$ [1, 2]. The lack of an inversion center, in the crystal structure, of an NCS superconductor makes parity an unconserved quantity. Therefore, the superconducting ground state of an NCS superconductor may exhibit a mixing of spin-singlet and spin-triplet pair states [3–11]. A parity mixed superconducting ground state can give rise to several anomalous superconducting properties, e.g. upper critical field exceeding the Pauli limit, nodes in the superconducting gap, a helical vortex state, and time-reversal symmetry breaking (TRSB).

Several NCS superconducting systems have been investigated to study the effects of broken inversion symmetry [12–28], but majority of them appear to show s-wave superconductivity. Theoretical predictions suggest that NCS superconductors are prime candidates to exhibit TRSB due to its admixed superconducting ground states. To date only a few NCS superconductors Re_6Zr [29], $LaNiC_2$ [30], SrPtAs [31] and La_7Ir_3 [32] have been reported to show TRSB. It is a rarely observed phenomena and apart from NCS superconductors, it has only been observed in a few unconventional superconductors e.g. Sr_2RuO_4 [33, 34], UPt_3 [35, 36], $PrPt_4Ge_{12}$ [37], $LaNiGa_2$ [38], and $Lu_5Rh_6Sn_{18}$ [39]. The discrepancy between theory, experiment and the possibility of realizing an unconventional superconducting state having TRSB in NCS superconductors are of great interest. To understand the superconducting mechanism, it is necessary to investigate new NCS superconducting systems by combining bulk measurements such as transport, magnetization, specific heat, etc and local probe techniques like muon spectroscopy. Muon spectroscopy

is one of the direct methods of detecting the unconventional superconducting ground state. This technique can accurately determine the temperature dependence of the magnetic penetration depth and the onset of TRSB in superconductors.

Here we report the properties of the superconducting state of a binary NCS compound (α-Mn structure) $Nb_{0.5}Os_{0.5}$, which has a superconducting transition at $T_c = 3.07$ K. Resistivity, magnetization, and specific heat measurements were carried out to explore the superconducting properties of $Nb_{0.5}Os_{0.5}$. μSR measurements in transverse-field (TF) and zero-field (ZF) were used to probe the flux line lattice and TRSB respectively.

2. Experimental details

The polycrystalline sample of $Nb_{0.5}Os_{0.5}$ was prepared by standard arc melting technique. The stoichiometric amounts of Nb (99.95%, Alfa Aesar) and Os (99.95%, Alfa Aesar) were placed on the water cooled copper hearth in an ultrapure argon gas atmosphere. The sample was inverted and remelted several times to ensure the sample homogeneity. There was a negligible weight loss during the sample synthesis. The sample was sealed inside an evacuated quartz tube and annealed at 1000 °C for 15 d in order to remove any thermal stresses if present in the sample. The phase analysis for $Nb_{0.5}Os_{0.5}$ was done using x-ray diffraction (XRD) at room temperature on an X'pert PANalytical diffractometer. The magnetization and ac susceptibility measurements were performed using a superconducting quantum interference device (MPMS 3, Quantum Design Inc.). The electrical resistivity and specific heat measurements were done using the physical property measurement system (PPMS, Quantum Design Inc.). The μSR measurements were carried out using the MuSR spectrometer at the ISIS facility, Rutherford Appleton Laboratory, Didcot, U.K. in both longitudinal and transverse geometries.

3. Results and discussion

3.1. Sample characterization

The powder x-ray diffraction pattern for $Nb_{0.5}Os_{0.5}$ was collected at room temperature. Rietveld refinement was performed using the High Score Plus Software. As observed from figure 1, the $Nb_{0.5}Os_{0.5}$ sample has no impurity phase. It can be indexed by cubic, noncentrosymmetric α-Mn structure (space group $I\bar{4}3m$, No. 217) with the lattice cell parameter $a = 9.765(3)$ Å. Also, the energy dispersive x-ray spectroscopy confirmed above-mentioned composition and showed that there are no other phases present in the sample to within the limits of these analysis techniques.

3.2. Normal and superconducting state properties

3.2.1. Electrical resistivity. The electrical resistivity measurement was done by the ac transport technique in the temperature range of $1.85\,\mathrm{K} \leqslant T \leqslant 300\,\mathrm{K}$ in zero field as displayed in figure 2. The superconducting transition temperature was

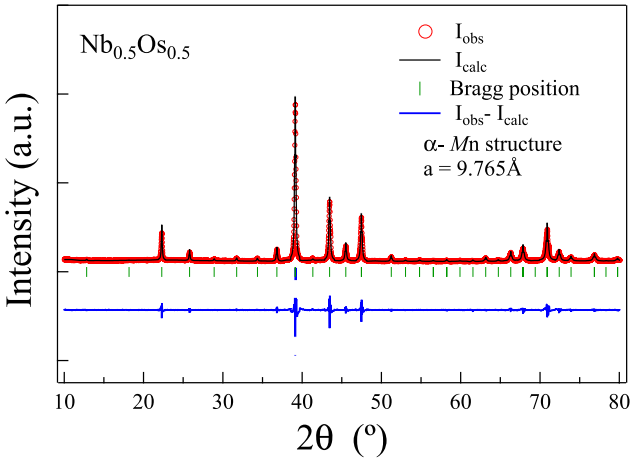

Figure 1. Powder XRD pattern for the $Nb_{0.5}Os_{0.5}$ sample recorded at room temperature using Cu K_α radiation. The red circles show the experimental data. The solid black line corresponds to Rietveld refinement to the pattern.

observed around $T_c = 3.1$ K (see inset: (a)). The normal state resistivity remains almost temperature independent up to the highest measured temperature, indicating that $Nb_{0.5}Os_{0.5}$ exhibit poor metallicity. Similar behavior was found in other compounds with the same structure and space group ($I\bar{4}3m$) [12–15, 40]. The resistivity measurements as a function of temperature were also done under different applied magnetic fields up to 3 T in a temperature range of 1.9 K to 12 K as shown in inset: (b) of figure 2. The superconducting transition temperature moves to the lower temperature with the increase in magnetic field, with the transition width becoming broader.

3.2.2. Magnetization. The magnetization measurement was done in zero-field cooling (ZFC) and field-cooled cooling (FCC) mode in an applied field of 1 mT. The strong diamagnetic signal due to the superconducting transition appears around $T_c^{onset} = 3.07$ K, as shown in figure 3(a). The value of $4\pi\chi$ at 1.8 K exceeds -1 due to the demagnetization effect. The magnetization measurement was done as a function of field at various temperatures to calculate the temperature dependence of the lower critical field $H_{c1}(T)$. Lower critical field is defined as the first deviation from linearity in low-field regions in M versus H curves (see inset figure 3(b)). The measurements were done upto a field range of 8 mT, at different temperatures from 1.9 K to 3 K. The main panel of figure 3(b) shows the $H_{c1}(T)$ plot, where the lower critical field decreases with the increase in temperature. The temperature variation of $H_{c1}(T)$ can be described by the Ginzburg–Landau (GL) formula

$$H_{c1}(T) = H_{c1}(0)\left(1 - \left(\frac{T}{T_c}\right)^2\right). \quad (1)$$

When fitted with the experimental data it yields $H_{c1}(0) = 3.06 \pm 0.05$ mT.

The temperature dependence of the upper critical field $H_{c2}(T)$ was obtained by measuring the field dependence of superconducting transition T_c in magnetization, ac susceptibility, resistivity, and specific heat measurements. It is evident

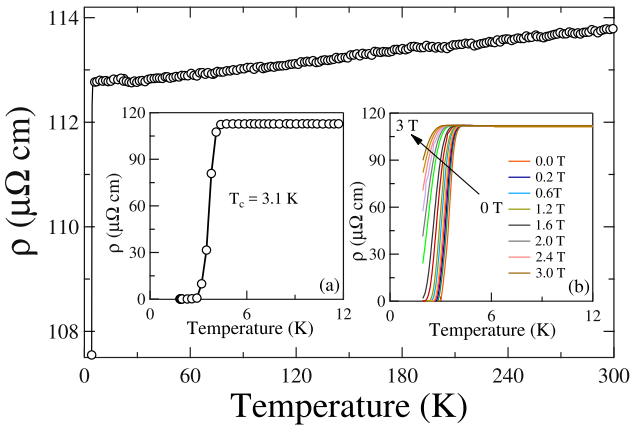

Figure 2. (a) The resistivity measurement $\rho(T)$ for $Nb_{0.5}Os_{0.5}$ taken in zero field in a temperature range of $1.85\,K \leqslant T \leqslant 300\,K$ showing poor metallicity. Inset: (a) the superconducting transition temperature is $T_c = 3.1$ K (b) $\rho(T)$ measurements done at several applied magnetic fields up to 3 T.

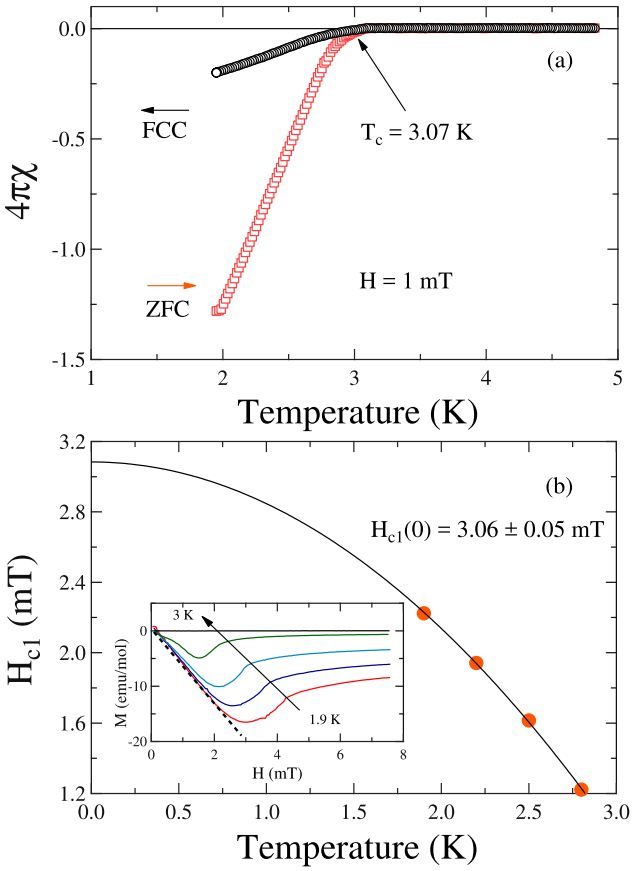

Figure 3. (a) The magnetization data for $Nb_{0.5}Os_{0.5}$ taken in 1 mT field shows the superconducting transition at $T_c = 3.07$ K. (b) The lower critical field H_{c1} was estimated to be 3.06 ± 0.05 mT. Inset: the magnetization curves as a function of applied magnetic field at various temperatures.

from figure 4 that H_{c2} vary linearly with the temperature and can possibly be best fitted by Ginzburg–Landau relation given by

$$H_{c2}(T) = H_{c2}(0)\frac{(1-t^2)}{(1+t^2)}, \tag{2}$$

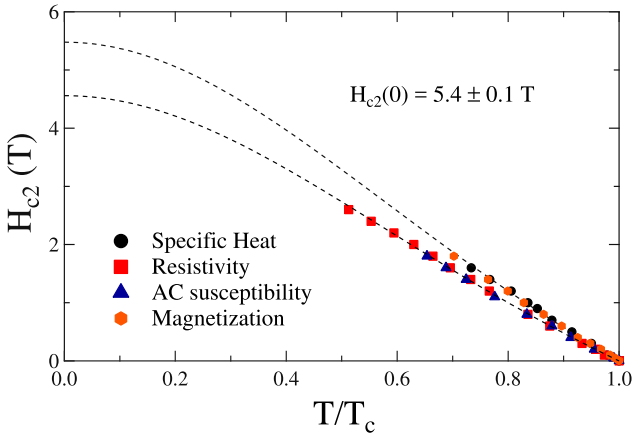

Figure 4. The upper critical field $H_{c2}(T)$ obtained from magnetization, ac susceptibility, resistivity, and specific heat measurements. The dotted lines show the GL fits, yielding $H_{c2}(0) \simeq 5.4 \pm 0.1$ T for $Nb_{0.5}Os_{0.5}$.

where $t = T/T_c$. By fitting above equation in the H_{c2}-T graph, the specific heat and magnetization measurements give $H_{c2}(0) \simeq 5.4 \pm 0.1$ T, whereas resistivity and ac susceptibility measurements give $H_{c2}(0) \simeq 4.6 \pm 0.1$ T.

$H_{c2}(0)$ can be used to estimate the Ginzburg Landau coherence length ξ_{GL} from the relation [41]

$$H_{c2}(0) = \frac{\Phi_0}{2\pi\xi_{GL}^2}, \tag{3}$$

where Φ_0 is the quantum flux $(h/2e)$. For $H_{c2}(0) \simeq 5.4 \pm 0.1$ T, we obtained $\xi_{GL}(0) = 78.12 \pm 0.72$ Å. For a type-II BCS superconductor in the dirty limit, the orbital limit of the upper critical field $H_{c2}^{orbital}(0)$ is given by the Werthamer–Helfand–Hohenberg expression [42, 43]

$$H_{c2}^{orbital}(0) = -0.693 T_c \left.\frac{-dH_{c2}(T)}{dT}\right|_{T=T_c}. \tag{4}$$

Using initial slope 2.10 ± 0.02 T K^{-1} from the H_{c2}-T phase diagram, $H_{c2}^{orbital}(0)$ in the dirty limit was estimated to be 4.46 ± 0.04 T. Within the α-model the Pauli limiting field is given by [44]

$$H_{c2}^{p}(0) = 1.86 T_c \left(\frac{\alpha}{\alpha_{BCS}}\right). \tag{5}$$

Using $\alpha = 1.81$ (from the specific heat measurement), it yields $H_{c2}^{p}(0) = 5.86$ T. The upper critical field $H_{c2}(0)$ calculated above is close to both the orbital limiting field and Pauli limiting field. Detailed investigations of the upper critical field in high quality single crystals of $Nb_{0.5}Os_{0.5}$ at low temperatures is highly desirable due to the possibility of enhanced upper critical field due to grain boundaries in polycrystalline samples. The Ginzburg Landau penetration depth $\lambda_{GL}(0)$ can be obtained from the $H_{c1}(0)$ and $\xi_{GL}(0)$ using the relation [41]

$$H_{c1}(0) = \frac{\Phi_0}{4\pi\lambda_{GL}^2(0)}\left(\ln\frac{\lambda_{GL}(0)}{\xi_{GL}(0)} + 0.12\right). \tag{6}$$

Using $H_{c1}(0) = 3.06$ mT and $\xi_{GL}(0) = 78.12$ Å, we obtained $\lambda_{GL}(0) \simeq 4774 \pm 50$ Å. The Ginzburg Landau parameter is given by the relation [41]

$$\kappa_{GL} = \frac{\lambda_{GL}(0)}{\xi_{GL}(0)}. \quad (7)$$

For $\xi_{GL}(0) = 78.12 \pm 0.72$ Å and $\lambda_{GL}(0) = 4774 \pm 50$ Å, it yields $\kappa_{GL} = 61.11 \pm 0.07$. This value of $\kappa_{GL} \gg \frac{1}{\sqrt{2}}$, indicating that $Nb_{0.5}Os_{0.5}$ is a strong type-II superconductor. Thermodynamic critical field H_c can be estimated from $\kappa_{GL}(0)$ and $H_{c2}(0)$ using the relation

$$H_c = \frac{H_{c2}}{\sqrt{2}\kappa_{GL}}, \quad (8)$$

which for $H_{c2} = 5.4 \pm 0.1$ T and $\kappa_{GL} = 61.11 \pm 0.07$ yields $H_c = 62.4 \pm 0.1$ mT.

3.2.3. Specific heat. The low temperature specific heat measurement $C(T)$ was taken in zero applied field. Figure 5(a) shows the C/T versus T^2 data in the temperature range 3 K $\leqslant T^2 \leqslant$ 100 K. The discontinuity in the specific heat data shows the onset of superconducting transition below $T_c = 3.0$ K, confirming the bulk superconductivity in $Nb_{0.5}Os_{0.5}$. The temperature dependence of the specific heat was done under different applied fields, where the increase of applied field suppresses the superconductivity, manifested by the shifting of transition temperature to lower temperature with the reduction in the specific heat jump as shown in the inset of figure 5(a). The normal state low temperature specific heat data above T_c can be fitted with the equation given below, where the extrapolation to the limit $T \to 0$ extracts the electronic and phononic contribution to the specific heat

$$\frac{C}{T} = \gamma_n + \beta_3 T^2 + \beta_5 T^4. \quad (9)$$

Here γ_n is the normal state Sommerfeld coefficient related to the electronic contribution to the specific heat whereas β_3 and β_5 are the coefficients related to the lattice contribution to the specific heat. The solid red line in the main panel of figure 5(a) shows the best fit to the data which yields $\gamma_n = 3.42 \pm 0.01$ mJ mol^{-1} K^{-2}, $\beta_3 = 0.039 \pm 0.002$ mJ mol^{-1} K^{-4}, and $\beta_5 = 0.205 \pm 0.004$ μJ mol^{-1} K^{-6}. The Debye temperature θ_D can be calculated from β_3 coefficient through formula

$$\theta_D = \left(\frac{12\pi^4 RN}{5\beta_3}\right)^{\frac{1}{3}}, \quad (10)$$

where R is the molar gas constant (=8.314 J mol^{-1} K^{-1}), gives $\theta_D = 367$ K. The Sommerfeld coefficient is proportional to the density of states $D_c(E_F)$ at the Fermi level given by

$$\gamma_n = \left(\frac{\pi^2 k_B^2}{3}\right) D_c(E_f), \quad (11)$$

where $k_B \approx 1.38 \times 10^{-23}$ J K^{-1}. Using $\gamma_n = 3.42 \pm 0.01$ mJ mol^{-1} K^{-2}, we obtained $D_c(E_F) = 1.45$ states/eV f.u.

The electron–phonon coupling constant can be calculated using the McMillan equation [45]

$$\lambda_{e-ph} = \frac{1.04 + \mu^* \ln(\theta_D/1.45T_c)}{(1 - 0.62\mu^*)\ln(\theta_D/1.45T_c) - 1.04}, \quad (12)$$

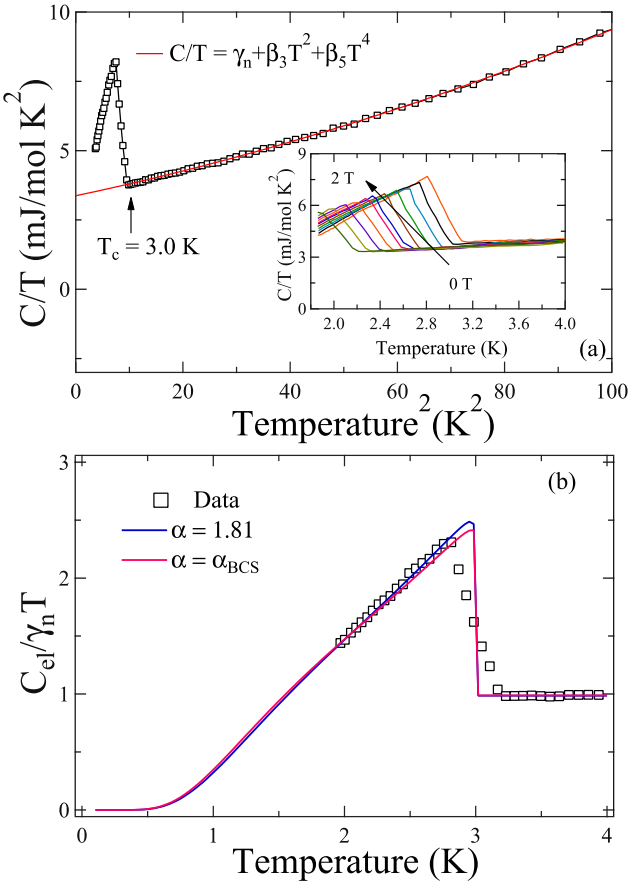

Figure 5. (a) The low temperature specific heat data above T_c is fitted to the Debye model shown by solid red line. Inset: the temperature dependence of the specific heat done at various applied fields, where jump size decreases with the increase in applied magnetic field. (b) The solid blue curve is theoretical prediction of the α model for $\alpha = \Delta(0)/k_B T_c = 1.81$ in $Nb_{0.5}Os_{0.5}$. The BCS prediction for $\alpha_{BCS} = 1.764$ is shown by solid red curve which deviates at temperature region around T_c.

where μ^* is the Coulomb repulsion parameter, typically given by $\mu^* = 0.13$ for many intermetallic superconductors. Using $T_c = 3.07$ K and $\theta_D = 367$ K for $Nb_{0.5}Os_{0.5}$, we obtained $\lambda_{e-ph} \simeq 0.53$. This value is comparable to other fully gapped NCS superconductors [12, 13, 46], suggesting that $Nb_{0.5}Os_{0.5}$ is a weakly coupled superconductor. Using the value of λ_{e-ph}, we have calculated the effective mass for the quasiparticles $m^* = 1.53\ m_e$ [47]. The electronic contribution to the specific heat can be calculated by subtracting the phononic contribution given by

$$C_{el}(T) = C(T) - (\beta_3 T^3 + \beta_5 T^5). \quad (13)$$

The magnitude of the specific heat jump for $Nb_{0.5}Os_{0.5}$ in $\Delta C_{el}/T_c$ data is 5.06 mJ mol^{-1} K^{-2}. The normalized specific heat jump $\frac{\Delta C_{el}}{\gamma_n T_c}$ is 1.48 for $\gamma_n = 3.42$ mJ mol^{-1} K^{-2}, which is close to the value for a BCS superconductor (=1.43) in the weak coupling limit. The temperature dependence of the normalized entropy S in the superconducting state for a single-gap BCS superconductor is given by

$$\frac{S}{\gamma_n T_c} = -\frac{6}{\pi^2}\left(\frac{\Delta(0)}{k_B T_c}\right)\int_0^\infty [f\ln(f) + (1-f)\ln(1-f)]\mathrm{d}y, \quad (14)$$

where $f(\xi) = [\exp(E(\xi)/k_BT) + 1]^{-1}$ is the Fermi function, $E(\xi) = \sqrt{\xi^2 + \Delta^2(t)}$, where ξ is the energy of normal electrons measured relative to the Fermi energy, $y = \xi/\Delta(0)$, $t = T/T_c$, and $\Delta(t) = \tanh[1.82(1.018((1/t) - 1))^{0.51}]$ is the BCS approximation for the temperature dependence of the energy gap. The normalized electronic specific heat is then calculated from the normalized entropy by

$$\frac{C_{el}}{\gamma_n T_c} = t\frac{d(S/\gamma_n T_c)}{dt}. \quad (15)$$

The C_{el} below T_c is described by equation (15) whereas above T_c its equal to $\gamma_n T_c$.

In the single-band α model, for systems where $\frac{\Delta C_{el}}{\gamma_n T_c} \neq 1.43$, the BCS parameter α_{BCS} is replaced by α which can be used as an adjustable parameter to fit the experimental superconducting specific heat data [44]. This parameter can be calculated using the equation

$$\frac{\Delta C_{el}}{\gamma_n T_c} = 1.426\left(\frac{\alpha}{\alpha_{BCS}}\right)^2. \quad (16)$$

Substituting the value of normalized specific heat jump $\Delta C_{el}/\gamma_n T_c = 1.48$ for our sample, we get $\alpha = 1.8$. The temperature dependence of single band α-model superconducting-state heat capacity $C_{el}(T)$ calculated for $\alpha = 1.81$ is shown by the solid blue curve in figure 5(b) together with that of the BCS prediction for $\alpha = \alpha_{BCS}$. It can be clearly seen that the curve for $\alpha = \alpha_{BCS}$ deviates around the temperature region near T_c, whereas it was much more improved for $\alpha = 1.81$. All the superconducting and normal state parameters are summarized in table 1.

3.2.4. Muon spin relaxation and rotation. The superconducting ground state of $Nb_{0.5}Os_{0.5}$ was further analyzed by μSR relaxation and rotation measurements. The zero-field muon spin relaxation (ZF-μSR) spectra was collected below ($T = 40$ mK) and above ($T = 3.5$ K) the transition temperature ($T_c = 3.07$ K) as displayed in figure 6. The absence of any oscillatory component in the spectra confirms that there are no atomic moments, generally associated with the ordered magnetic structure. In the absence of atomic moments, muon-spin relaxation in zero field is given by the Gaussian Kubo–Toyabe (KT) function [48]

$$G_{KT}(t) = \frac{1}{3} + \frac{2}{3}(1 - \sigma_{ZF}^2 t^2)\exp\left(\frac{-\sigma_{ZF}^2 t^2}{2}\right), \quad (17)$$

where σ_{ZF} accounts for the relaxation due to static, randomly oriented local fields associated with the nuclear moments at the muon site. The spectra well described by the function

$$A(t) = A_1 G_{KT}(t)\exp(-\Lambda t) + A_{BG}, \quad (18)$$

where A_1 is the initial asymmetry, Λ is the electronic relaxation rate, and A_{BG} is the time-independent background contribution from the muons stopped in the sample holder. By fitting both the ZF-μSR spectra (figure 6) with the equation (18), yields the similar set of parameters within the sensitivity of the instrument as shown in table 2. This leads to the conclusion that the time-reversal symmetry is preserved in $Nb_{0.5}Os_{0.5}$ within the detection limit of μSR.

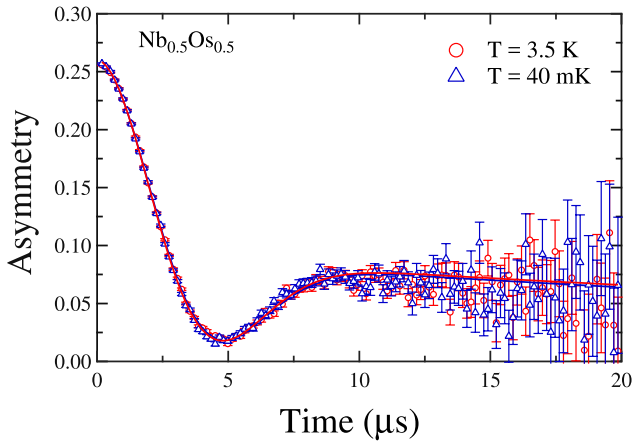

Figure 6. Zero field μSR spectra collected below (40 mK) and above (3.5 K) the superconducting transition temperature. The solid lines are the fits to Gaussian KT function given in equation (18).

Transverse-field muon spin rotation (TF-μSR) measurements were done to gain information on the superconducting gap structure of $Nb_{0.5}Os_{0.5}$. Asymmetry spectra was recorded above (3.5 K) and below (0.1 K) the transition temperature T_c in a transverse field of 30 mT as shown in figure 7. The TF-μSR precession signal were fitted using an oscillatory decaying Gaussian function

$$G_{TF}(t) = A_1\exp\left(\frac{-\sigma^2 t^2}{2}\right)\cos(w_1 t + \phi) + A_2\cos(w_2 t + \phi), \quad (19)$$

where w_1 and w_2 are the frequencies of the muon precession signal and background signal respectively, ϕ is the initial phase offset and σ is the Gaussian muon-spin relaxation rate. Figure 7(a) shows the signal in the normal state where depolarization rate is small, attributed to homogeneous field distribution throughout the sample. The significant depolarization rate in the superconducting state shown in the figure 7(b) is due to the flux line lattice (FLL) in the mixed state of the superconductor, which gives rise to the inhomogeneous field distribution. The depolarization arising due to the static fields from the nuclear moments σ_N is assumed to be temperature independent and adds in quadrature to the contribution from the field variation across the flux line lattice σ_{FLL}:

$$\sigma^2 = \sigma_N^2 + \sigma_{FLL}^2. \quad (20)$$

The muon-spin relaxation rate in the superconducting state σ_{FLL} is related to the London magnetic penetration depth λ and thus to the superfluid density n_s by the equation

$$\frac{\sigma_{FLL}(T)}{\sigma_{FLL}(0)} = \frac{\lambda^{-2}(T)}{\lambda^{-2}(0)}. \quad (21)$$

For an s-wave BCS superconductor in the dirty limit, the temperature dependence of the London magnetic penetration depth is given by

$$\frac{\lambda^{-2}(T)}{\lambda^{-2}(0)} = \frac{\Delta(T)}{\Delta(0)}\tanh\left[\frac{\Delta(T)}{2k_BT}\right], \quad (22)$$

Table 1. Normal and superconducting properties of $Nb_{0.5}Os_{0.5}$.

Parameter	Unit	Value
T_c	K	3.07
$H_{c1}(0)$	mT	3.06
$H_{c2}(0)$	T	5.4
$H_c(0)$	mT	62.4
$H_{c2}^{orbital}(0)$	T	4.46
$H_{c2}^{P}(0)$	T	5.86
ξ_{GL}	Å	78.12
λ_{GL}	Å	4774
κ_{GL}		61
γ	mJ mol^{-1} K^{-2}	3.42
β	mJ mol^{-1} K^{-4}	0.039
θ_D	K	367
λ_{e-ph}		0.53
$D_c(E_f)$	states/ev f.u	1.45
$\Delta C_{el}/\gamma_n T_c$		1.48
$\Delta(0)/k_B T_c$		1.81

Table 2. Parameters extracted from the fits using the KT function to the zero-field μSR data collected above and below T_c for $Nb_{0.5}Os_{0.5}$.

Parameter	Above T_c	Below T_c
A_1	0.250 ± 0.005	0.253 ± 0.005
σ_{ZF}	0.361 ± 0.003	0.365 ± 0.001
Λ	0.031 ± 0.003	0.034 ± 0.004
$A_{BG}(0)$	0.011 ± 0.001	0.012 ± 0.003

where $\Delta(T) = \Delta_0 \delta(T/T_c)$. The temperature dependence of the gap in the BCS approximation is given by the expression $\delta(T/T_c) = \tanh[1.82(1.018((T_c/T) - 1))^{0.51}]$. By combining equations (20)–(22), a model was obtained for a dirty limit single-gap s-wave superconductor, where $\sigma(T)$ above T_c is equal to σ_N and below T_c is given by equation (23) which contain contributions from both σ_N and σ_{FLL}.

$$\sigma(T) = \sqrt{\sigma_{FLL}^2(0)\frac{\Delta^2(T)}{\Delta^2(0)}\tanh^2\left[\frac{\Delta(T)}{2k_BT}\right] + \sigma_N^2}. \quad (23)$$

The temperature dependence of muon depolarization rate σ was collected in an applied field of 30 mT as shown in figure 8. The depolarization rate σ remains temperature independent up to T_c attributing to random nuclear magnetic moments, then after T_c, σ increases due to the formation of well-ordered FLL. The best fit to the $\sigma(T)$ data were obtained with the single-gap BCS model (equation (23)) shown by the solid blue line in figure 8, where we have obtained $\sigma_N = 0.366 \pm 0.002$ μs^{-1}, $\sigma(0) = 0.444 \pm 0.001$ μs^{-1}, and $\Delta(0) = 0.50 \pm 0.02$ meV. The value of $\alpha = \Delta(0)/k_BT_c = 1.89$ is close to the value ($\alpha = 1.81$) obtained from the low temperature specific heat measurement. Thus, the TF-μSR measurements together with the specific heat measurement confirm that $Nb_{0.5}Os_{0.5}$ is a s-wave superconductor.

The GL penetration depth $\lambda_\mu(0)$ at $T = 0$ K can be directly calculated ($\sigma_{FLL}(0) = 0.251 \pm 0.001$ μs^{-1}) from muon measurements by the relation [49, 50]

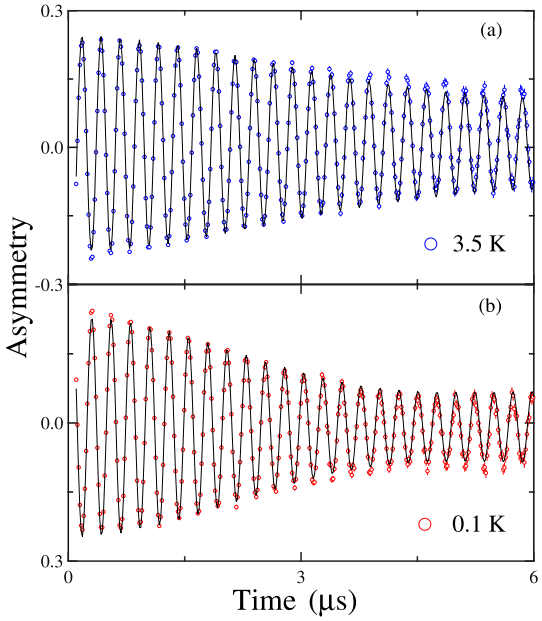

Figure 7. Representative TF μSR signals collected at (a) 3.5 K and (b) 0.1 K in an applied magnetic field of 30 mT. The solid lines are fits using equation (19).

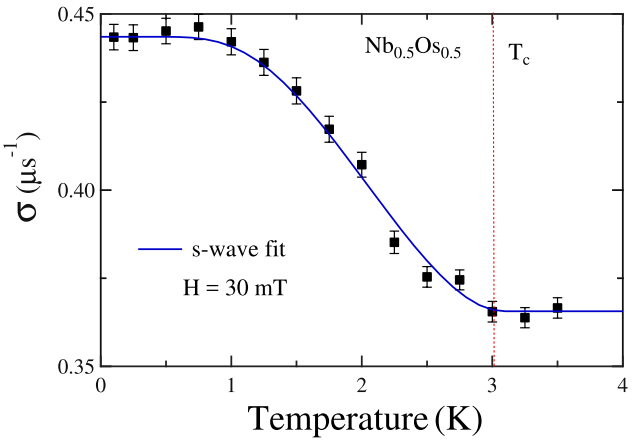

Figure 8. The temperature dependence of the muon-spin relaxation rate $\sigma(T)$ collected at an applied field of 30 mT. The solid blue line shows the s-wave fit for a dirty limit superconductor using equation (23).

$$\frac{\sigma_{FLL}^2(0)}{\gamma_\mu^2} = 0.00371\frac{\Phi_0^2}{\lambda_\mu^4(0)}, \quad (24)$$

where $\gamma_\mu/2\pi = 135.53$ MHz T^{-1} is the muon gyromagnetic ratio and Φ_0 is the magnetic flux quantum. The value of GL penetration depth $\lambda_\mu(0)$ is 6538 ± 13 Å. The estimated value is higher than the $\lambda_{GL}(0)$ calculated earlier, which could be due to the dirty limit superconductivity in $Nb_{0.5}Os_{0.5}$.

Uemura *et al* showed in 1991 that the superconductors can be classified into a conventional/unconventional superconductor [51, 52] based on the ratio of the transition temperature (T_c) to the Fermi temperature (T_F). It was shown that the unconventional, exotic superconductors fall in the range of $0.01 \leqslant \frac{T_c}{T_F} \leqslant 0.1$. The Fermi temperature can be calculated using the relation

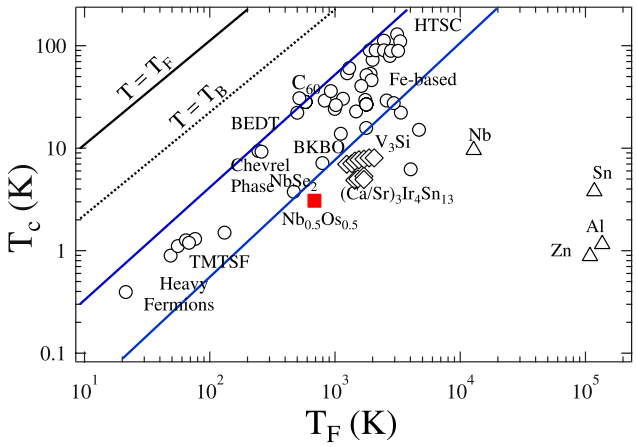

Figure 9. The Uemura plot showing the superconducting transition temperature T_c versus the effective Fermi temperature T_F, where $Nb_{0.5}Os_{0.5}$ is shown as a solid red square. Other data points plotted between the blue solid lines are the different families of unconventional superconductors.

$$k_B T_F = \frac{\hbar^2}{2}(3\pi^2)^{2/3}\frac{n_s^{2/3}}{m_e[1+\lambda_{e-ph}]}, \qquad (25)$$

where n_s is the density of paired electrons and λ_{e-ph} is the electron–phonon coupling constant. Using the Sommerfeld coefficient for $Nb_{0.5}Os_{0.5}$ [27, 53], we have calculated the number density of electrons $n_e = 2.94 \times 10^{30}$ m^{-3}. The estimated value of l (0.56 Å) $\ll \xi_0$ (14091 Å), confirming that the superconductivity in $Nb_{0.5}Os_{0.5}$ is in the dirty-limit as predicted earlier. The density of paired electrons will be given by $n_s \simeq n_e \frac{l}{\xi_0} = 1.17 \times 10^{26}$ m^{-3}. The above result is verified from the magnetic penetration depth λ_μ calculated from the muon analysis, where the density of paired electrons is given by $n_s = \frac{m_e(1+\lambda_{e-ph})}{\mu_0 e^2 \lambda_\mu^2} \simeq 1.01 \times 10^{26}$ m^{-3}.

Using the value of n_s in equation (25), it yields $T_F = 662$ K, giving the ratio $\frac{T_c}{T_F} = 0.0046$, just outside the range of unconventional superconductors as shown by a solid red square in figure 9, where blue solid lines represent the band of unconventional superconductors. A similar result is obtained if we express the superfluid density in term of the muon spin-relaxation rate $\sigma(0) \propto \lambda(0)^{-2} \propto \rho_s(0)$ as in the original Uemura plot.

4. Conclusion

The sample of $Nb_{0.5}Os_{0.5}$ was prepared by standard arc-melting technique. XRD analysis confirms the phase purity and cubic, NCS α-Mn structure (space group no.217) with lattice cell parameter $a = 9.765(3)$ Å. The transport, magnetization, and specific heat measurements confirm type-II, s-wave superconductivity in $Nb_{0.5}Os_{0.5}$ having transition temperature $T_c = 3.07$ K. The upper and lower critical fields estimated to be $H_{c1} \simeq 3.06$ mT and $H_{c2} \simeq 5.4$ T respectively. The TF-μSR measurements further confirm s-wave superconductivity. The ZF-μSR measurements confirm that time-reversal symmetry is preserved in $Nb_{0.5}Os_{0.5}$ within the detection limit of μSR. In order to understand the superconducting ground state of NCS compounds, it is clearly important to search for new NCS superconductors.

Acknowledgments

RPS acknowledges Science and Engineering Research Board, Government of India for the Young Scientist Grant YSS/2015/001799 and Ramanujan Fellowship through Grant No. SR/S2/RJN-83/2012. We thank ISIS, STFC, UK for the muon beamtime and Newton Bhabha funding to conduct the μSR experiments.

ORCID iDs

R P Singh https://orcid.org/0000-0003-2548-231X

References

[1] Bauer E, Hilscher G, Michor H, Paul C, Scheidt E W, Gribanov A, Seropegin Y, Noël H, Sigrist M and Rogl P 2004 *Phys. Rev. Lett.* **92** 027003
[2] Bauer E and Sigrist M 2012 *Non-Centrosymmetric Superconductor: Introduction and Overview* (Heidelberg: Springer)
[3] Gor'kov L P and Rashba E I 2001 *Phys. Rev. Lett.* **87** 037004
[4] Yip S K 2002 *Phys. Rev.* B **65** 144508
[5] Samokhin K V, Zijlstra E S and Bose S K 2004 *Phys. Rev.* B **69** 094514
[6] Sergienko I A and Curnoe S H 2004 *Phys. Rev.* B **70** 214510
[7] Frigeri P A, Agterberg D F, Koga A and Sigrist M 2004 *Phys. Rev. Lett.* **92** 097001
[8] Fujimoto S 2005 *Phys. Rev.* B **72** 024515
[9] Fujimoto S 2006 *J. Phys. Soc. Japan* **75** 083704
[10] Fujimoto S 2007 *J. Phys. Soc. Japan* **76** 051008
[11] Sigrist M, Agterberg D F, Frigeri P A, Hayashi N, Kaur R P, Koga A, Milat I, Wakabayashi K and Yanase Y 2007 *J. Magn. Magn. Mater.* **310** 536
[12] Karki A B, Xiong Y M, Haldolaarachchige N, Stadler S, Vekhter I, Adams P W, Young D P, Phelan W A and Chan J Y 2011 *Phys. Rev.* B **83** 144525
[13] Lue C S, Liu H F, Kuo C N, Shih P S, Lin J-Y, Kuo Y K, Chu M W, Hung T-L and Chen Y Y 2013 *Supercond. Sci. Technol.* **26** 055011
[14] Chen B, Guo Y, Wang H, Su Q, Mao Q, Du J, Zhou Y, Yang J and Fang M 2016 *Phys. Rev.* B **94** 024518
[15] Singh D, Hillier A D, Thamizhavel A and Singh R P 2016 *Phys. Rev.* B **94** 054515
[16] Chen J, Salamon M B, Akutagawa S, Akimitsu J, Singleton J, Zhang J L, Jiao L and Yuan H Q 2011 *Phys. Rev.* B **83** 144529
[17] Kuroiwa S, Saura Y, Akimitsu J, Hiraishi M, Miyazaki M, Satoh K H, Takeshita S and Kadono R 2008 *Phys. Rev. Lett.* **100** 097002
[18] Biswas P K, Lees M R, Hillier A D, Smith R I, Marshall W G and Paul D M 2011 *Phys. Rev.* B **84** 184529
[19] Klimczuk T, Ronning F, Sidorov V, Cava R J and Thompson J D 2007 *Phys. Rev. Lett.* **99** 257004
[20] Qi Y, Guo J, Lei H, Xiao Z, Kamiya T and Hosono H 2014 *Phys. Rev.* B **89** 024517

[21] Karki A B, Xiong Y M, Vekhter I, Browne D, Adams P W, Young D P, Thomas K R, Chan J Y, Kim H and Prozorov R 2010 *Phys. Rev.* B **82** 064512
[22] Shibayama T, Nohara M, Aruga Katori H, Okamoto Y, Hiroi Z and Takagi H 2007 *J. Phys. Soc. Japan* **76** 073708
[23] Wakui K, Akutagawa S, Kase N, Kawashima K, Muranaka T, Iwahori Y, Abe J and Akimitsu J 2009 *J. Phys. Soc. Japan* **78** 034710
[24] Anand V K, Hillier A D, Adroja D T, Strydom A M, Michor H, McEwen K A and Rainford B D 2011 *Phys. Rev.* B **83** 064522
[25] Smidman M, Hillier A D, Adroja D T, Lees M R, Anand V K, Singh R P, Smith R I, Paul D M and Balakrishnan G 2014 *Phys. Rev.* B **89** 094509
[26] Kase N and Akimitsu J 2009 *J. Phys. Soc. Japan* **78** 044710
[27] Anand V K, Britz D, Bhattacharyya A, Adroja D T, Hillier A D, Strydom A M, Kockelmann W, Rainford B D and McEwen K A 2014 *Phys. Rev.* B **90** 014513
[28] Khan M A *et al* 2016 *Phys. Rev.* B **94** 144515
[29] Singh R P, Hillier A D, Mazidian B, Quintanilla J, Annett J F, Paul D M, Balakrishnan G and Lees M R 2014 *Phys. Rev. Lett.* **112** 107002
[30] Hillier A D, Quintanilla J and Cywinski R 2009 *Phys. Rev. Lett.* **102** 117007
[31] Biswas P K *et al* 2013 *Phys. Rev.* B **87** 180503
[32] Barker J A T, Singh D, Thamizhavel A, Hillier A D, Lees M R, Balakrishnan G, Paul D M and Singh R P 2015 *Phys. Rev. Lett.* **115** 267001
[33] Luke G M *et al* 1998 *Nature* **394** 558
[34] Xia J, Maeno Y, Beyersdorf P T, Fejer M M and Kapitulnik A 2006 *Phys. Rev. Lett.* **97** 167002
[35] Luke G M, Keren A, Le L P, Wu W D, Uemura Y J, Bonn D A, Taillefer L and Garrett J D 1993 *Phys. Rev. Lett.* **71** 1466
[36] de Reotier P D, Huxley A, Yaouanc A, Flouquet J, Bonville P, Impert P, Pari P, Gubbens P C M and Mulders A M 1995 *Phys. Lett.* A **205** 239
[37] Maisuradze A, Schnelle W, Khasanov R, Gumeniuk R, Nicklas M, Rosner H, Leithe-Jasper A, Grin Y, Amato A and Thalmeier P 2010 *Phys. Rev.* B **82** 024524
[38] Hillier A D, Quintanilla J, Mazidian B, Annett J F and Cywinski R 2012 *Phys. Rev. Lett.* **109** 097001
[39] Bhattacharyya A, Adroja D T, Quintanilla J, Hillier A D, Kase N, Strydom A M and Akimitsu J 2015 *Phys. Rev.* B **91** 060503
[40] Cirillo C, Fittipaldi R, Smidman M, Carapella G, Attanasio C, Vecchione A, Singh R P, Lees M R, Balakrishnan G and Cuoco M 2015 *Phys. Rev.* B **91** 134508
[41] Tinkham M 1996 *Introduction to Superconductivity* 2nd edn (New York: McGraw-Hill)
[42] Helfand E and Werthamer N R 1966 *Phys. Rev.* **147** 288
[43] Werthamer N R, Helfand E and Hohenberg P C 1966 *Phys. Rev.* **147** 295
[44] Johnston D C 2013 *Supercond. Sci. Technol.* **26** 115011
[45] McMillan W L 1968 *Phys. Rev.* **167** 331
[46] Isobe M, Masao A and Shirakawa N 2016 *Phys. Rev.* B **93** 054519
[47] Grimvall G 1976 *Phys. Scr.* **14** 63
[48] Hayano R S, Uemura Y J, Imazato J, Nishida N, Yamazaki T and Kubo R 1979 *Phys. Rev.* B **20** 850
[49] Sonier J E, Brewer J H and Kiefl R F 2000 *Rev. Mod. Phys.* **72** 769
[50] Brandt E H 1988 *Phys. Rev.* B **37** 2349
[51] Hashimoto K *et al* 2012 *Science* **336** 1554
[52] Uemura Y J *et al* 1989 *Phys. Rev. Lett.* **62** 2317
[53] Kittel C 2005 *Introduction to Solid State Physics* 8th edn (New York: Wiley)